



Integration of a thermochemical energy storage system in a Rankine cycle driven by concentrating solar power: Energy and exergy analyses

Ugo Pelay, Lingai Luo, Yilin Fan, Driss Stitou, Cathy Castelain

► To cite this version:

Ugo Pelay, Lingai Luo, Yilin Fan, Driss Stitou, Cathy Castelain. Integration of a thermochemical energy storage system in a Rankine cycle driven by concentrating solar power: Energy and exergy analyses. *Energy*, 2019, 167, pp.498-510. 10.1016/j.energy.2018.10.163 . hal-02364774

HAL Id: hal-02364774

<https://hal.science/hal-02364774>

Submitted on 27 Nov 2020

HAL is a multi-disciplinary open access archive for the deposit and dissemination of scientific research documents, whether they are published or not. The documents may come from teaching and research institutions in France or abroad, or from public or private research centers.

L'archive ouverte pluridisciplinaire **HAL**, est destinée au dépôt et à la diffusion de documents scientifiques de niveau recherche, publiés ou non, émanant des établissements d'enseignement et de recherche français ou étrangers, des laboratoires publics ou privés.

Integration of a Thermochemical Energy Storage System in a Rankine Cycle Driven by Concentrating Solar Power: Energy and Exergy Analyses

Ugo PELAY^a, Lingai LUO^{a,*}, Yilin FAN^a, Driss STITOU^b, Cathy CASTELAIN^a

^a Laboratoire de Thermique et Energie de Nantes (LTEN), CNRS UMR 6607, Université de Nantes,
La Chantrerie, Rue Christian Pauc, BP 50609, 44306 Nantes Cedex 03, France

^b Laboratoire PROcédures, Matériaux et Energie Solaire (PROMES), CNRS UPR 8521, Tecnosud,
Rambla de la thermodynamique, 66100 Perpignan, France

Abstract:

This paper proposes and investigates novel concepts on the integration of a thermochemical energy storage (TCS) system in a concentrating solar power (CSP) plant. The TCS material used is calcium oxide reacting with water and the power cycle studied is a Rankine cycle driven by CSP. Firstly, three integration concepts on the coupling of the TCS system with the Rankine cycle are proposed, including the thermal integration concept, the mass integration concept and the double turbine concept. Then, an energy analysis is performed to determine and compare the theoretical overall energy efficiency of the proposed concepts. After that, an exergy analysis is also carried out for the selected integration concepts so as to evaluate and compare the overall exergy efficiency of the installation with TCS integration.

The results show that the turbine integration concept has the highest overall energy efficiency (0.392), followed by the thermal integration concept (0.358) and the mass integration concept (0.349) under ideal conditions with 11 h of charging and 13 h of discharging. The energy storage density using calcium hydroxide as the storage media is estimated to be about 100 kWh \cdot t⁻¹. Exergy analysis results also indicate that the turbine integration concept seems to be the best option under the tested conditions.

Keywords: Thermal energy storage (TES); Thermochemical; Rankine cycle; Concentrating solar power (CSP); Integration concept; Calcium hydroxide; exergy analysis

Declarations of interest: none

* Corresponding author. Tel.: +33 240683167; E-mail address: lingai.luo@univ-nantes.fr

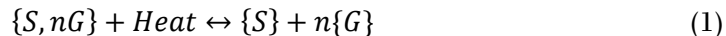
40 **1. Introduction**

41
42 The increasing energy demand, the environmental protection issue and the national energy
43 independence all over the world call for researches aiming at more efficient use of renewable energy
44 such as solar energy. Among various solar energy technologies, the Concentrating Solar Power (CSP)
45 plants are expected to play an important role in the energetic scenarios owing to its advantages in
46 terms of high efficiency, low operating cost and good scale-up potential [Cáceres 2013; Zhang 2013;
47 Dunham 2014; Balghouthi 2016]. According to IRENA [2016], the CSP deployment would reach
48 44 GW in the reference scenario (Remap 2030). It is estimated that the CSP would contribute up to
49 11.3% of the electricity production in the year 2050, with 954 GW of installed capacity [IEA 2014;
50 del Río 2018].

51
52 One of the advantages of CSP technology is the possibility of integrating a thermal energy
53 storage (TES) function, permitting the production of electricity any time when it is the most needed
54 and valuable, whether during the peak hours, nights, or cloudy intervals [Zhang 2016; Dowling
55 2017; Alva 2018]. To do this, a TES system at high temperature should be designed and installed
56 properly between the solar field and a power cycle. Although adding a TES system usually increases
57 the investment cost of the CSP plant, it improves significantly its adaptability and dispatchability.
58 CSP plants (existing or under construction) having TES systems at high temperature are
59 summarized in recent reviews [e.g., Tian 2013; Kuravi 2013; Pelay 2017a; b]. The storage capacity
60 in terms of discharging time is generally between 3 to 8 hours, and recently up to 15 hours
61 (Gemasolar, Spain) aiming at round-the-clock electricity production driven by solar energy [Dunn
62 2012].

63
64 The most commonly used storage technology is based on the sensible heat storage, in which
65 the thermal energy is stored/released by raising/decreasing the temperature of a storage material.
66 This technology is the most mature and deeply investigated, with a wide variety of both liquid (e.g.,
67 pressurized water, molten salt, mineral oil, etc.) and solid (e.g., sand, rock, cast iron, etc.) materials
68 being used for CSP applications [Gil 2010; Tiskatine 2017]. Some recent developments are also
69 reported, such as on the use of industrial wastes or by-products [Ortega-Fernández 2015; Gutierrez
70 2016], chloride salts [Myers 2016], lithium coupled with molten salts [Cabeza 2015], or solid particles
71 [Zhang 2017a; Calderón 2018]. However, their limited energy density (usually between 60
72 kWh_{th}·m⁻³ (200 °C-300 °C) for sand, rock and mineral oil, and 150 kWh_{th}·m⁻³ for cast iron (200 °C-
73 400 °C) [Fernandes 2012]) increases significantly the size of TES systems. Latent heat storage
74 materials such as Phase Change Materials (PCMs) are also proposed for CSP applications owing to
75 their higher storage capacity [Gil 2010; Pitié 2013; Sharma 2015; Zhang 2017b; Chirino 2018]. But
76 their small thermal conductivity (commonly 0.2 - 0.8 W·m⁻¹·K⁻¹) usually limits the heat transfer,
77 resulting in very slow charging and discharging processes [Nithyanandam 2015]. Some new
78 advances on the effective encapsulation of PCMs [Zhang 2014; Parrado 2015] as well as the
79 enhancement of thermal conductivity are summarized in recent papers [Xu 2015; Liu 2016; Alva
80 2018].

82 Besides the sensible and latent heat storage technologies, the thermochemical storage (TCS)
83 is a promising solution for its highest storage capacity (up to 10 times greater than latent storage
84 [Pardo 2014a]), wide accessible temperature range and long storage duration at ambient
85 temperature [Prieto 2016]. This technology is mainly based on reversible chemical reactions (e.g.,
86 gas-solid) involving absorbing or releasing a large amount of reaction heat:
87



88
89 The charging stage uses solar energy for the decomposition of $\{S, nG\}$ associated with the
90 condensation of the gas while the discharging stage brings the solid and gas into contact for heat
91 release by the exothermic reaction. TCS material candidates at a medium or high temperature (300–
92 1000 °C) for CSP application include metallic hydrides, carbonates system, hydroxides system,
93 redox system, ammonia system and organic system [Kuravi 2013]. Their mains characteristics,
94 advantages/disadvantages and experimental feedback are reviewed and summarized in [Pelay
95 2017a].
96

97 Beyond the testing of new TCS materials [e.g., Deutsch 2017; Valverde 2017;
98 Bagherisreshki 2018] and proper reactor designs [e.g., Álvarez De Miguel 2013; Schmidt 2017;
99 Wokon 2017; Pan 2017] and pilot scale testing [Tescari 2017a; b], the TCS system must be coupled
100 in a proper way with the vapor generator of the power cycle (e.g., Rankine cycle) in a CSP plant.
101 However, relatively little attention seems to be given to this integration issue. Recently, Cabeza et
102 al. [2017] proposed a new concept of consecutive TCS reactions (either one cycle or two coupled
103 cycles) and its implementation in CSP plants, with the purpose of eliminating reversibility problems
104 and therefore improving the overall efficiency. Ortiz et al. [2017] proposed possible integration
105 schemes of calcium looping (CaO-CaCO_3) for power production by direct or indirect means. Their
106 results showed highest plant efficiencies up to 45–46% using a closed carbon dioxide Brayton power
107 cycle. Noteworthy is the very recent work of Schmidt and Linder [2017], in which an integration
108 option of the TCS system into a CSP plant has been proposed and analyzed. Their analysis showed
109 that a storage efficiency up to 87% might be reached when the required steam production during
110 discharge is thermally integrated into the Rankine steam cycle.
111

112 From the above literature survey, one may find that the research on how to integrate the
113 TCS system to the power cycle of the CSP plant is insufficient. Actually, it is an essential issue for
114 the implementation and application of TCS technology, calling for deeper and extensive
115 investigations. The main objectives and originalities of this paper are therefore threefold: (1) to
116 propose various novel integration concepts of TCS system into the Rankine cycle driven by CSP,
117 for both charging and discharging stages; (2) to perform a detailed energy analysis of the proposed
118 integrated concepts and to evaluate impacts of various influencing factors on the overall energy
119 efficiency of the CSP plant; and (3) to discuss and compare the second law efficiency of the proposed
120 integration concepts through an exergy analysis.
121

122 This paper is organized as follows. In section 2, the selected gas-solid reaction and material
123 are briefly introduced and the key issue on how to manage the water vapor from the TCS reactor is

124 identified. Three novel TCS integration concepts (thermal integration, mass integration and turbine
125 integration) are proposed and described in section 3. The performance modelling of the three
126 integration concepts based on energy analysis is presented and discussed in section 4. Section 5
127 provides an exergy analysis of the integration concepts. Finally, main conclusions and future work
128 are summarized in section 6.

129

130 **2. Thermochemical reaction and its operation**

131

132 In this section, we briefly introduce the selected gas-solid reaction and materials, as well as
133 the identified key issues for the integration of TCS unit into the Rankine cycle.

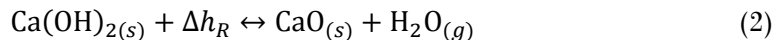
134

135 *2.1. Reaction used as TCS storage media*

136

137 Various hydrates and hydroxides have been proposed as potential TCS materials, as
138 summarized in some latest papers [e.g., Aydin 2015; André 2016; Liu 2016; Prieto 2016; Pelay 2017a;
139 Zhang 2016]. Among them, the CaO/H₂O couple has been deeply studied with a great amount of
140 experimental feedback [e.g., Azpiazu 2003; Michel 2012; Schabe 2013a; b; Pardo 2014b; Yan 2016;
141 2017; Sakellariou 2017]. It is found to be a pertinent candidate as TCS material for CSP application
142 with various features, including for high-temperature use (450~600 °C), good reversibility,
143 operating pressure close to the atmospheric pressure, low material cost, environment-friendly and
144 high energy density (about 3 GJ·m⁻³), etc. As a result, it is selected *a priori* for this conceptual study.
145 The reaction formula is shown in Eq. (2).

146



147

148 For a reaction temperature at 500 °C, the equilibrium pressure equals to 0.1 MPa (1 bar).
149 Under this condition, the reaction heat (Δh_R) is found to be 104 kJ·mol(CaO)⁻¹=5774.56 kJ·Kg(H₂O)⁻¹
150 ¹ [Schaube, 2011].

151

152

153 *2.2. Management of the water vapor from the TCS reactor*

154

155 The integration of TCS reactor in a solar power plant is a so-called passive concept in which
156 the storage medium (CaO) is kept motionless and heated-up or cooled-down by the circulation of a
157 heat transfer fluid (HTF) [Pelay 2017a]. When used as TCS material in a CSP plant, water vapor at
158 high temperature produced by the decomposition during the charging stage should preferably be
159 condensed to saturated liquid and stored in a separate reservoir at ambient pressure (0.1 MPa).
160 Hence the required volume for the storage unit is greatly reduced. Meanwhile, the superheated
161 steam (500 °C) contains a significant amount of thermal energy, a part of which is possible to be
162 recovered so as to increase the overall efficiency of the whole system, as shown in Fig. 1a. Instead
163 of condensing the water vapor directly at the outlet of the TCS reactor by an additional condenser,
164 alternative energy valorization options are actually available, either to produce extra electricity
165 through an additional turbine or to preheat the steam of the Rankine cycle.

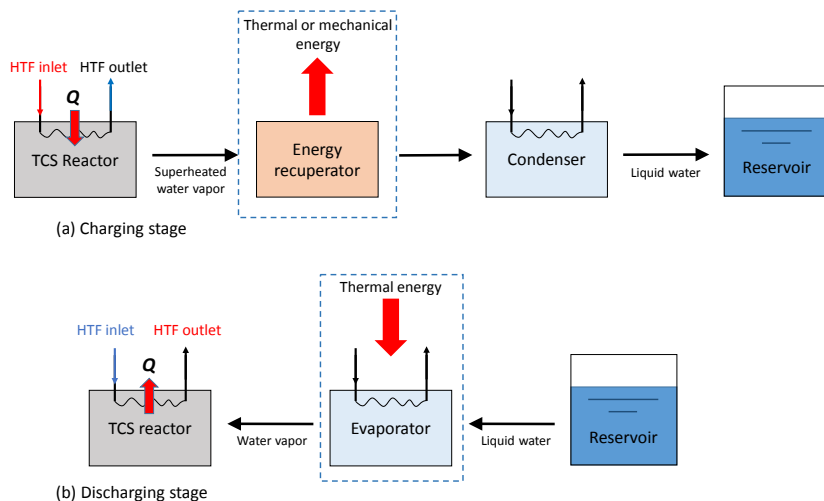
166

167 During the discharging stage, the exothermic synthesis happens when CaO and water vapor
 168 are in contact. Supposing that the CSP plant is driven only by solar energy, it is necessary to find a
 169 heat source to vaporize water stored previously in the liquid form through an evaporator, as shown
 170 in Fig. 1b. This heat source should have a higher temperature than that of liquid water to be
 171 evaporated (e.g., 100 °C at 1 bar).

172

173 As a result, the positioning of TCS reactor in the whole system and the way of managing
 174 water vapor are key issues for an energy-efficient integration of TCS unit into the Rankine cycle.
 175 Different integration concepts shown in the following section will highlight the options proposed for
 176 these key points.

177



178

179 Figure 1. Management of water vapor as a key issue for energy-efficient TCS integrations into the Rankine cycle. (a)
 180 charging stage; (b) discharging stage.

181

182

183 3. TCS integration concepts

184

185 In this section, we shall firstly present a conventional regenerative Rankine cycle driven by
 186 CSP without storage as a reference case [Moran, 2003]. Then, three novel integration concepts of
 187 TCS unit into the Rankine cycle are proposed and described, named as thermal integration, mass
 188 integration and turbine integration.

189

190

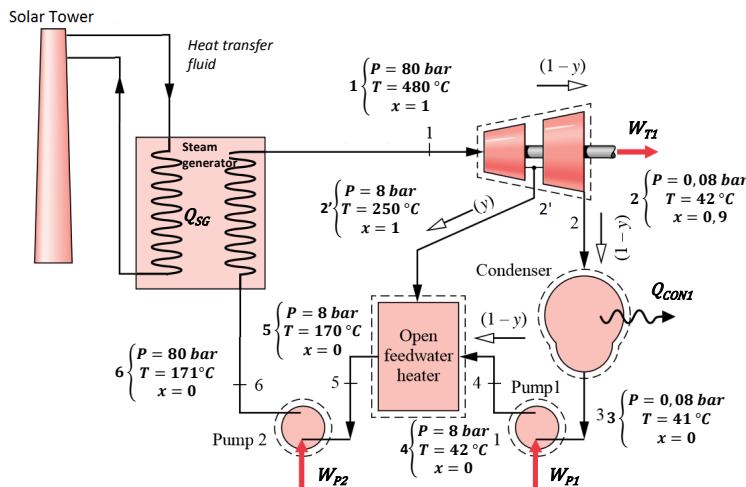
191 3.1. Conventional Rankine cycle without TES

192

193 Figure 2 shows a representative schematic view of the conventional regenerative Rankine
 194 cycle driven by CSP. The main components in this cycle include a steam generator, a turbine, a
 195 condenser, an open feedwater heater and pumping and piping accessories. Solar energy is firstly
 196 absorbed by the solar receiver at the top of solar tower and transferred to the HTF. This amount of
 197 thermal energy is then utilized in converting water contained in generator (point 6) into superheated
 198 steam at the suitable pressure and temperature (point 1). The superheated steam then flows through

199 the turbine. While doing work in the turbine, the pressure of steam is reduced. The steam leaving
 200 the turbine (point 2) passes through the condenser and is condensed into liquid at low pressure for
 201 recycling. An open (or direct-contact) feedwater heater serves as a mixing chamber where the steam
 202 extracted from the turbine (point 2') mixes with the feedwater leaving the pump (point 4). Ideally,
 203 the mixture leaves the heater as the saturated liquid at the heater pressure (point 5). This steam
 204 regeneration configuration usually enhances the thermal efficiency of the Rankine cycle at the cost
 205 of lower electricity production rate due to steam extraction.

206



207
 208 Figure 2. Schematic view of a conventional regenerative Rankine cycle driven by CSP without TES [Moran 2003]

209

210

211 3.2. Concept 1: Thermal integration (Thermal Int.)

212

213 The Thermal Int. concept is shown in Fig. 3. The added TCS unit comprises of a TCS reactor,
 214 a water reservoir, a second condenser and two heat exchangers. There are three fluid circuits in the
 215 integrated system: the solar circuit as energy supply, the principal Rankine circuit for power
 216 generation and the TCS circuit for energy storage. Note that although the working fluids are
 217 identical as pure water or steam, the principal Rankine circuit and the TCS circuit are independent
 218 of each other without direct mass contact or exchange. Hence, this concept is named as Thermal
 219 Int. because there is only heat exchange between the TCS circuit and the Rankine circuit.

220

221 During the charging stage (Fig. 3a), the HTF (e.g., pressurized air or molten salt) from the
 222 solar tower offers the steam generator sufficient amount of thermal energy to run the principal
 223 Rankine cycle. Meanwhile, it heats the $\text{Ca}(\text{OH})_2$ reactive salts in the TCS reactor up to 500 °C at 1
 224 bar to initiate the decomposition. The water vapor generated in the TCS reactor is partially
 225 condensed in the heat exchanger 1, then completely condensed in the condenser 2 and finally be
 226 stored as the saturated liquid (100 °C, 1 bar) in a separate water reservoir. The sensible and latent
 227 heat released by the water vapor will be used to preheat the working fluid of the principal Rankine
 228 circuit via heat exchanger 1. The CaO reaction product (and subsequent reactant) remains in the
 229 TCS reactor. This integration concept permits the steady operation of the principal Rankine circuit
 230 for power production and the TES in parallel.

231

During the discharging stage (Fig. 3b) when solar energy is not available, the liquid water stored in the reservoir is firstly heated up and vaporized by the high temperature steam extracted from the turbine of the principal Rankine circuit via the heat exchanger 2. The saturated vapor (100°C , 1 bar) enters then into the TCS reactor and reacts with the CaO for the synthesis of $\text{Ca}(\text{OH})_2$. The heat released from this exothermic reaction in the TCS reactor runs the principal Rankine cycle steadily under the same operational conditions (temperature, pressure and steam mass flow-rate) as during the charging stage. In this case, the TCS reactor also serves as the steam generator.

The positive aspect of this concept is that it is technically simple to implement whereas the disadvantage is that a separate reservoir is required to store the liquid water resulting from the TCS reaction, implying a higher capital cost.

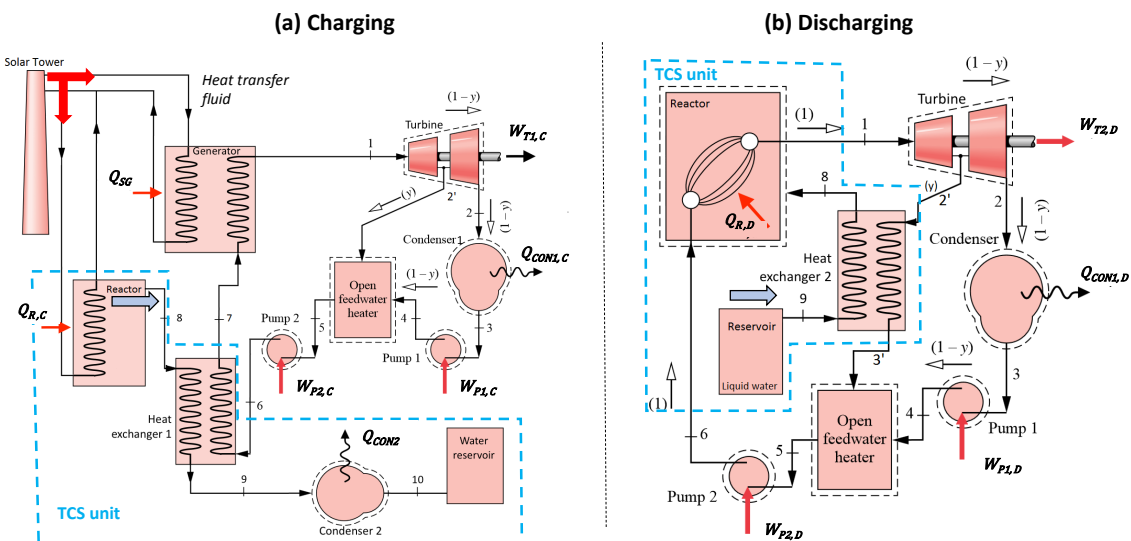


Figure 3. Schematic view of the thermal integration concept. (a) charging stage; (b) discharging stage [Luo 2016].

3.3. Concept 2: Mass integration (Mass Int.)

The Mass Int. concept is shown in Fig. 4. Compared to the conventional Rankine cycle as shown in Fig. 2, a TCS unit is added including a TCS reactor, a second condenser, a throttle valve, a third pump and two heat exchangers. There are still three fluid circuits in the installation: the solar circuit, the principal Rankine circuit and the TCS circuit. But different from the above-mentioned Thermal Int. concept, the principal Rankine circuit and the TCS circuit are coupled and share the same working fluid (pure water or steam) with mass exchange. As a result, this concept is named as Mass Int.

During the charging stage (Fig. 4a), the water vapor generated in the TCS reactor is partially condensed in the heat exchanger 1, depressurized by the throttle valve, completely condensed in the condenser 2 and finally stored as the saturated water (41°C , 0.008 MPa) in the water reservoir shared with the principal Rankine circuit. The sensible and latent heat released by the common

water vapor will be used to preheat the working fluid of the Rankine cycle via the heat exchanger 1 located upstream of the steam generator.

During the discharging stage (Fig. 4b), the liquid water stored in the reservoir will be pressurized by pump 3 and then evaporated by exchanging heat with the extracted steam via the heat exchanger 2. The saturated vapor (100°C , 0.1 MPa) enters the TCS reactor and reacts with the CaO reactive salts stored inside. Again, the TCS reactor serves as the steam generator to run the Rankine cycle steadily under the same operational conditions as during the charging stage.

The Mass Int. concept seems less interesting than the Thermal Int. concept because more components are required for the TCS unit, implying higher capital costs. Moreover, the mixing of working fluids between the principal Rankine circuit and the TCS circuit could bring further technical difficulties because of the massive fines formation. An efficient filtration system (e.g., sintered metal fiber or ceramic filters [Smolders 2000]) may have to be implemented for dust removal to prevent the eventual damage of the turbine. A special design of the TCS reactor coupled with metal filter may also be considered [Schmidt 2017].

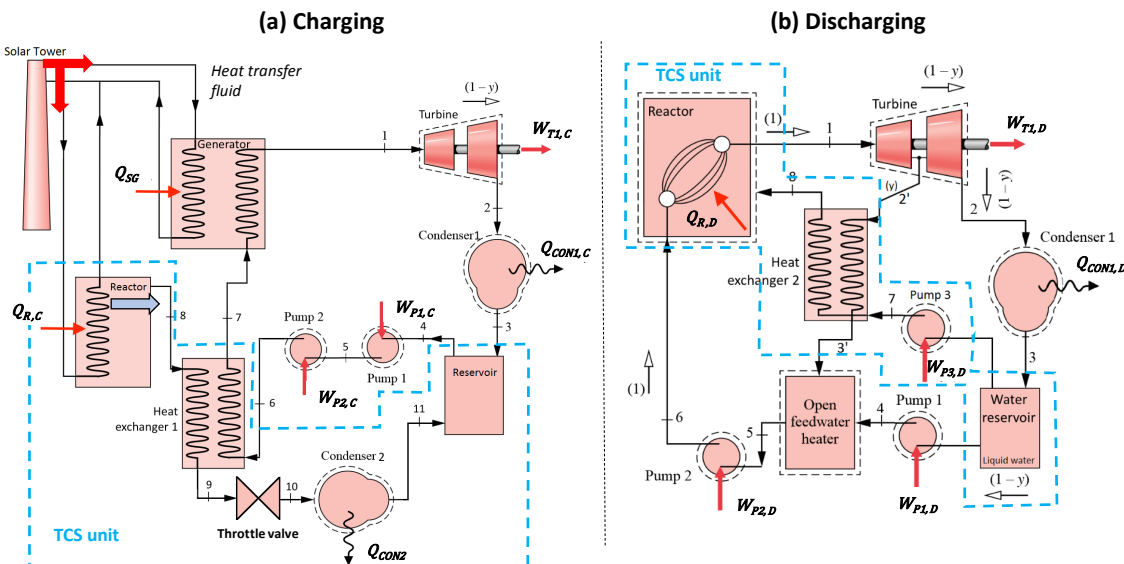


Figure 4. Schematic view of the mass integration concept. (a) charging stage; (b) discharging stage [Luo 2016].

3.4. Concept 3: Turbine integration (Turbine Int.)

Figure 5 presents a schematic view of the Turbine Int. concept. Additional components of the TCS unit include a TCS reactor, a second turbine, a second condenser, a third pump, a water reservoir and a heat exchanger. The principal Rankine circuit and the TCS circuit are completely independent of each other during the charging stage (no heat or mass exchange) and thermally coupled during the discharging stage.

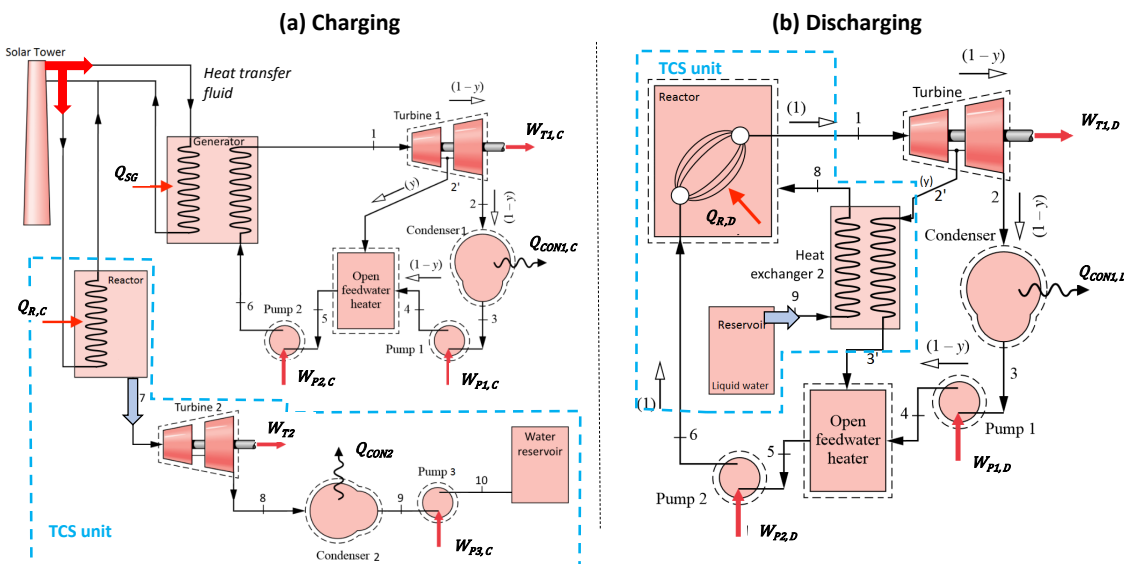
During the charging stage (Fig. 5a), the water vapor generated in the TCS reactor passes through the turbine 2, condensed in the condenser 2 and finally stored as the sub-saturated water

(41.5 °C, 0.1 MPa) in a water reservoir. A part of its thermal energy is valorized as power production via the second turbine. The integration concept for the discharging stage (Fig. 5b) is the same as that of Thermal Int. concept, in which water stored in the reservoir will be evaporated by exchanging heat with the extracted steam via the heat exchanger 2.

297

298 The main feature of this concept is the additional power production in parallel of the one
299 provided by the principal Rankine circuit during the charging stage. However, the implementation
300 of this second turbine, which is partially used only during the charging stage, implies higher capital
301 cost for the CSP plant.

302



303
304 Figure 5. Schematic view of the turbine integration concept. (a) charging stage; (b) discharging stage [Luo 2016].
305
306

307 4. Energy analysis of different TCS integration concepts

308

309 This section presents a detailed energy analysis of three proposed concepts of TCS
310 integration into the Rankine cycle of a CSP plant. Firstly, the performance modelling of each
311 individual components and of the system as a whole will be described under ideal operating
312 conditions (as indicated in Fig. 1). Then a parametric study on various influencing factors will be
313 performed so as to identify appropriate functioning points for different integration concepts towards
314 performance comparison.

315

316

317 4.1. Performance modelling

318

319 The performance analysis is based on the conservation of mass and energy. To simplify the
320 calculation, the following assumptions are made, while the influences of certain factors will be
321 discussed through the parametric study in the later section. Note that the solar receiver and the
322 solar tower have not been included in the current analysis. It is supposed that the solar field provides

323 the required amount of thermal energy for the power production of the Rankine cycle and the TES
324 during the charging stage.

325

- 326 (A1) Steady-state operation;
327 (A2) Isentropic compression and expansion processes ($\eta_{isen}=1$);
328 (A3) Evaporation and condensation at constant pressure;
329 (A4) Negligible heat loss; negligible pressure drop of piping system;
330 (A5) During the charging, the water vapor at 500 °C and 0.1 MPa is released from the TCS
331 reactor; during the discharging, the saturated vapor (100 °C, 0.1 MPa) is injected into
332 the TCS reactor; 100% conversion rate of the TCS reactor ($\gamma=1$), no mass leakage
333 during the storage;
334 (A6) The power output rate from the turbine of the principal Rankine circuit $W_{T1} = 100 \text{ MW}_{\text{el}}$.

Table I. Mass and energy conservation equations for the performance modelling of Rankine cycle with or without TCS integration.

		Reference case	Thermal Int.		Mass Int.		Turbine Int.		Note
Component	charging		discharging		charging	discharging	charging	discharging	
Principal Rankine circuit	Turbine 1 (T1)			$T_{T1}^{in} = 480 \text{ }^{\circ}\text{C}$, $P_{T1}^{in} = 8.0 \text{ MPa}$; $P_{T1}^{out} = 0.008 \text{ MPa}$; $P_{T1}^{ext} = 0.08 \text{ MPa}$					N1
				$W_{T1,C(D)} = m_{Rankine,C(D)}[(h_{T1}^{in} - h_{T1}^{ext}) + (1 - y_{C(D)}) (h_{T1}^{ext} - h_{T1}^{out})]$ (3)					
				$\eta_{T1,C(D)} = \frac{h_{T1}^{ext} - h_{T1}^{in}}{h_{T1,isen}^{ext} - h_{T1}^{in}} = \frac{h_{T1}^{out} - h_{T1}^{ext}}{h_{T1,isen}^{out} - h_{T1}^{ext}}$ (4)					
	Condenser 1 (CON1)			$Q_{CON1,C(D)} = m_{Rankine,C(D)}(1 - y_{C(D)})(h_{CON1}^{in} - h_{CON1}^{out})$ (5)					N2
				$P_{CON1}^{in} = P_{CON1}^{out}$					
	Pump 1 (P1)			$W_{P1,C(D)} = m_{Rankine,C(D)}(1 - y_{C(D)})(h_{P1}^{out} - h_{P1}^{in})$ (6)					N3
TCS circuit	Feedwater heater (FH)			$y_{C(D)} h_{FH}^{in1} + (1 - y_{C(D)}) h_{FH}^{in2} = h_{FH}^{out}$ (8)		-		(8)	
				$P_{FH}^{in1} = P_{FH}^{in2} = P_{FH}^{out}$ (9)				(9)	
	Pump 2 (P2)			$W_{P2,C(D)} = m_{Rankine,C(D)}(h_{P2}^{out} - h_{P2}^{in})$ (10)					N4
				$\eta_{P2,C(D)} = \frac{h_{P2,isen}^{out} - h_{P2}^{in}}{h_{P2}^{out} - h_{P2}^{in}}$ (11)					
	Steam generator (SG)			$Q_{SG} = m_{Rankine}(h_{SG}^{out} - h_{SG}^{in})$ (12)		(12)		(12)	
				$P_{SG}^{in} = P_{SG}^{out}$ (13)		(13)		(13)	
TCS circuit	TCS reactor (R)	-	$\gamma Q_{R,C} = m_{TCS,C} \Delta h_R$ (14)	$Q_{R,D} = \gamma m_{TCS,D} (h_{R,D}^{out} - h_{R,D}^{in})$ (15)		(14)	(15)	(14)	N5
	Condenser 2 (CON2)	-	$Q_{CON2} = m_{TCS,C} (h_{CON2}^{in} - h_{CON2}^{out})$ (18)			(18)		(18)	
			$P_{CON2}^{in} = P_{CON2}^{out} = 0.1 \text{ MPa}$ (19)		$P_{CON2}^{in} = P_{CON2}^{out} = 0.008 \text{ MPa}$ (20)			(20)	
TCS circuit	Heat exchanger 1 (HX1)	-	$\frac{h_{HX1,Rankine}^{out}}{m_{TCS,C}} = (h_{HX1,TCS}^X - m_{Rankine,C}^{in}) + h_{HX1,TCS}^Y$ (21)			(21)		-	N6
			$h_{HX1,TCS}^{out} = \frac{m_{Rankine,C}}{m_{TCS,C}} (h_{HX1,Rankine}^Y - h_{HX1,Rankine}^{in}) + h_{HX1,TCS}^X$ (22)			(22)		-	
	Heat exchanger 2 (HX2)	-	-	$m_{TCS,D} (h_{HX2,TCS}^{out} - h_{HX2,TCS}^{in}) =$			(23)	-	(23)

			$y_D m_{Rankine,D} (h_{HX2,Rankine}^{in} - h_{HX2,Rankine}^{out})$ (23)					
Water reservoir (WS)	-	Saturated water at 0.1 MPa		Saturated water at 0.008 MPa		Sub-saturated water (41.5 °C) at 0.1 MPa		N7
Throttle valve (TV)	-	-	-	$h_{TV}^{in} = h_{TV}^{out}$ $P_{TV}^{in} = 0.1 \text{ MPa}; P_{TV}^{out} = 0.008 \text{ MPa}$ (24)	-	-	-	
Pump 3 (P3)	-	-	-	-	$P_{P3}^{in} = 0.008 \text{ MPa}; P_{P3}^{out} = 0.1 \text{ MPa}$ $W_{P3,C(D)} = m_{TCS,C(D)} (h_{P3}^{out} - h_{P3}^{in})$ (25) $\eta_{P3,C(D)} = \frac{h_{P3,isen}^{out} - h_{P3}^{in}}{h_{P3}^{out} - h_{P3}^{in}}$ (26)	-	-	
Turbine 2 (T2)	-	-	-	-	$P_{T2}^{out} = 0.008 \text{ MPa}$ $W_{T2} = m_{TCS} (h_{T2}^{in} - h_{T2}^{out})$ (27) $\eta_{T2} = \frac{h_{T2}^{out} - h_{T2}^{in}}{h_{T2,isen}^{out} - h_{T2}^{in}}$ (28)	-	-	
Overall energy efficiency of the installation	$\frac{\eta_o}{W_{T1}-W_{P1}-W_{P2}} = \frac{Q_{SG}}{Q_{RG}}$ (29)	$\eta_o = \frac{(W_{T1,C}-W_{P1,C}-W_{P2,C})H_C + (W_{T1,D}-W_{P1,D}-W_{P2,D})H_D}{(Q_{SG}+Q_{R,C})H_C}$ (30)	$\eta_o = \frac{(W_{T1,C}-W_{P1,C}-W_{P2,C})H_C + (W_{T1,D}-W_{P1,D}-W_{P2,D}-W_{P3,D})H_D}{(Q_{SG}+Q_{R,C})H_C}$ (31)	$\eta_o = \frac{(W_{T1,C}+W_{T2,C}-W_{P1,C}-W_{P2,C}-W_{P3,C})H_C + (W_{T1,D}-W_{P1,D}-W_{P2,D})H_D}{(Q_{SG}+Q_{R,C})H_C}$ (32)				N8

N1: saturated steam at the turbine extraction; $y_c=0$ for Mass Int. concept.

N2: $y_c=0$ for Mass Int. concept.

N3: saturated water at the inlet of P1; $y_c=0$ for Mass Int. concept.

N4: $T_{P2}^{in} = 41.6 \text{ °C}$ for the discharging stage of Thermal Int. and Mass Int.; saturated water for the rest of concepts.

N5: H_C and H_D are the number of operating hours for charging and for discharging, respectively; γ is the conversion rate of the TCS reactor; Eq. (15) implies that a portion of reaction heat is consumed to heat the saturated vapor (100 °C 0.1 MPa) to the equilibrium temperature of reaction (500 °C 0.1 MPa).

N6: X and Y are intermediate points located at the hot side (TCS) and cold side (Rankine) of the HX1, respectively; saturated steam at X point; $T_{HX1,TCS}^{out} - T_{HX1,Rankine}^Y = 5 \text{ °C}$ (pinch point of HX1).

N7: no thermal losses during the storage period.

N8: Q_{SG} and $Q_{R,C}$ are the amount of heat provided by the HTF; the solar field (solar receiver) is not included in the analysis.

324 Mass and energy conservation equations for the individual components and for the whole
 325 system of different concepts are listed in Table 1. Values of thermodynamic properties of water and
 326 steam are determined referring to NIST-JANAF Thermochemical Tables [Chase, 1998]. Detailed
 327 values of main status points of the Rankine cycle with or without TCS integration may be found in
 328 the supplementary material of this paper.

329

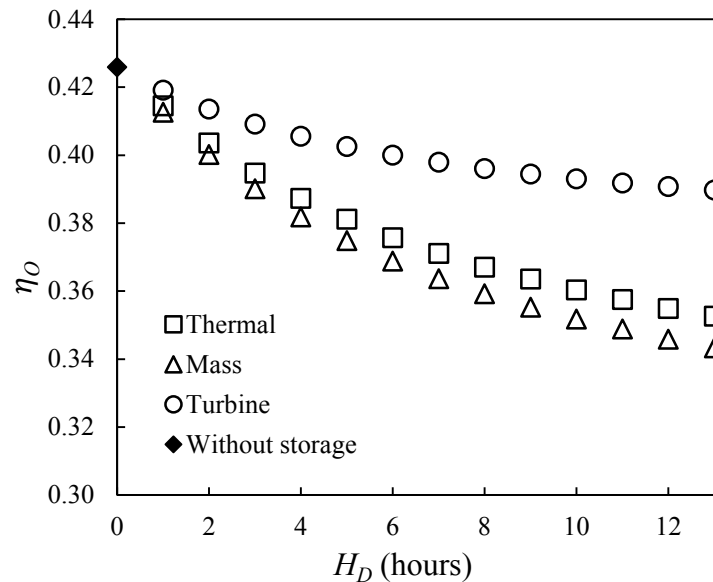
330 Following this modeling procedure, the global performance of three proposed integration
 331 concepts is analyzed and compared with that of conventional Rankine cycle without storage
 332 (reference case). The charging/discharging scenarios examined cover a large variety of operation
 333 possibilities, for the charging time (H_C) varying from 1 hour to 12 hours and the discharging time
 334 (H_D) varying from 0 hour to 13 hours.

335

336 Figure 6 shows the overall energy efficiency of the installation (η_0) for different integration
 337 concepts under the above-mentioned ideal operational conditions, for various charging (Fig. 6b) and
 338 discharging (Fig. 6a) scenarios. η_0 is defined as the total net output work of the Rankine cycle
 339 (during charging and discharging) divided by all the energy absorbed from the HTF of the solar
 340 circuit (during charging), as indicated in Eqs. 29-32.

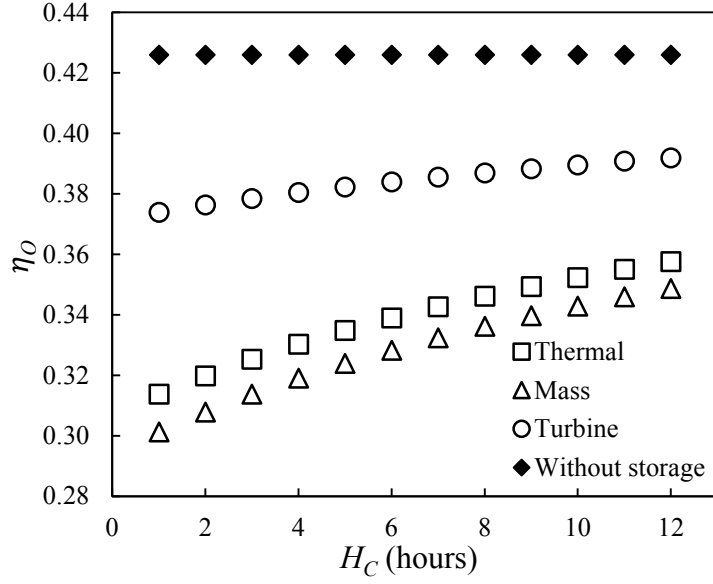
341

342 It can be observed from Fig. 6a that for a given charging time ($H_C=11$ h), the values of η_0
 343 with TCS integration are lower than that of the reference case ($\eta_{0, ref}=0.42$) without TCS. This can
 344 be explained by the loss of a part of the energy contained in the superheated vapor produced by the
 345 TCS reactor during the charging hours. A large part of the energy is recovered/valorized via the heat
 346 exchanger 1 (Thermal Int. and Mass Int.) and via the turbine 2 (Turbine Int.). But still, a small part
 347 is lost in the condenser 2. It can also be observed in Fig. 6a that the Turbine Int. has the highest η_0
 348 while the Mass Int. has the lowest. This difference becomes more important with the increasing
 349 number of discharging hours. Figure 6b shows that for a given discharging time ($H_D=12$ h), the η_0
 350 of all concepts of TCS integration increases when the number of charging hours (H_C) increases. It
 351 seems that a low H_D/H_C ratio is favorable to achieve high values η_0 when TCS unit is integrated into
 352 the CSP plant.



(a)

353



(b)

Figure 6. Overall energy efficiency of the installation (η_0) for different integration concepts under ideal operational conditions. (a) different number of discharging hours ($H_c=11$ h); (b) different number of charging hours ($H_d=12$ h).

However, longer discharging shows clear advantages in terms of higher dispatchability and higher total power output. As shown in Fig. 7, the daily power output of Turbine Int. could reach 3010 MWh_{el} for 11 hours of charging and 13 hours of discharging (round-the-clock operation), which is augmented by a factor of 2.7 compared to that of the reference case without storage (only 11 hours daily production). The benefits of TCS integration into the CSP plant are therefore highlighted. In real world practice, the operation strategy of the TCS unit certainly deserves detailed investigations by taking various influencing factors into account (e.g., climate condition for charging hour, electricity demand profile for the discharging hour, hourly electricity price for techno-economic consideration, etc.).

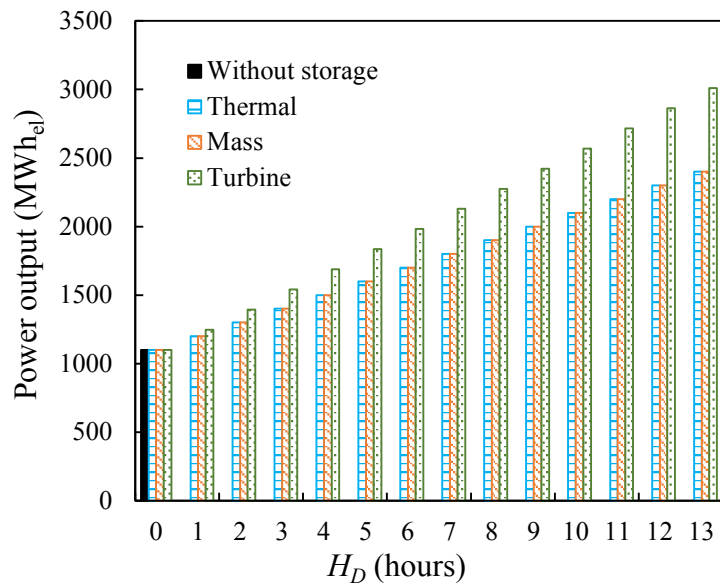


Figure 7. Power production of CSP plants as a function of the number of discharging hours ($H_c=11$ h).

372

373 4.2. Parametric study

374

375 It should be noted that in section 4.1, the overall energy efficiency is estimated under ideal
 376 conditions, neglecting all the losses. From the viewpoint of real-world engineering, it is necessary to
 377 evaluate the real performances when actual operational conditions differ from the ideal one. In this
 378 section, the impacts of various influencing factors on the overall energy efficiency of the plant are
 379 analyzed and discussed. The studied parameters include the isentropic efficiency of turbomachines
 380 (turbines and pumps), the steam temperature at the inlet of turbine 1 and the global efficiency of
 381 the TCS reactor. Note that to evaluate the separate effect of a certain parameter, only the concerned
 382 parameter is varied while others are kept as the ideal operational conditions used for performance
 383 modelling in section 4.1.

384

385 • Isentropic efficiency of turbomachines η_{isen}

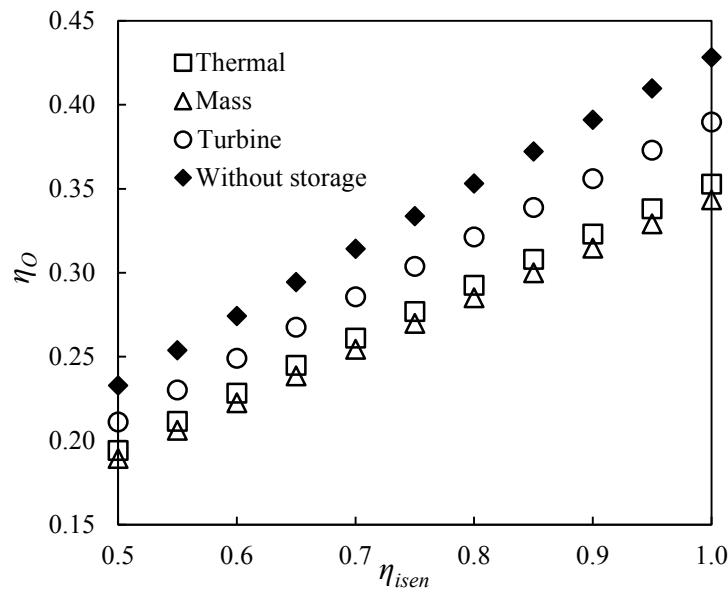
386

387 We define the parameter η_{isen} as the isentropic efficiency of turbine or pumps, to represent
 388 non-isentropic compression or expansion processes. Different values of η_{isen} from 0.5 to 1.0 are tested
 389 and added to the relevant energy conservation equations for turbines and pumps to determine the
 390 values of main status points of the cycle. Note that for simplification purpose, the equal value of
 391 η_{isen} is assumed for all turbomachines.

392

393 Figure 8 represents the variation of η_o values for different concepts as a function of the
 394 isentropic efficiency of turbomachines. The negative effect of non-isentropic compression/expansion
 395 of turbines and pumps can be clearly observed. Each 10% decrement of η_{isen} results in about 4.2-
 396 4.5% reduction in the η_o .

397



398

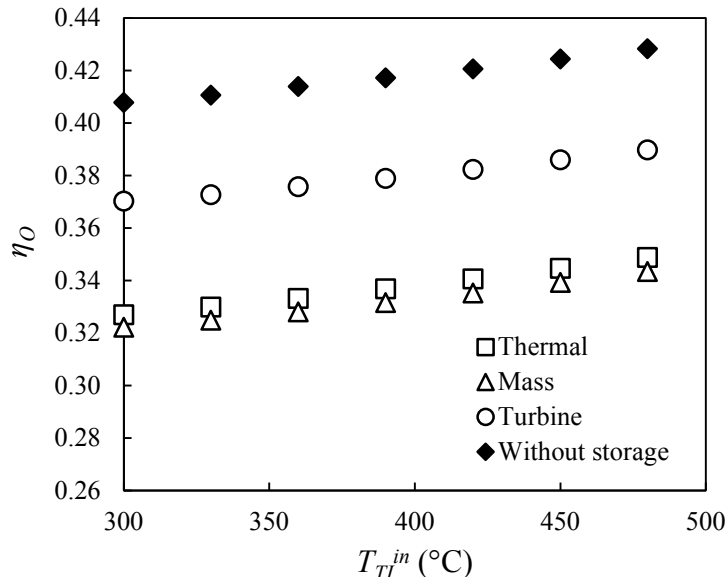
399 Figure 8. Overall energy efficiency (η_o) as a function of the isentropic efficiency (η_{isen}) of turbines and pumps ($H_c=11$ h;
 400 $H_d=13$ h).

401

402
403
404
405
406
407
408
409
410

- Steam temperature at the inlet of turbine 1

Increasing the steam temperature at the inlet of turbine 1 (T_{T1}^{in}) means the increased temperature of the superheated steam at the outlet of the steam generator (during charging) and the TCS reactor (during discharging). This usually leads to the augmented turbine work output. It may be observed from Fig. 9 that the η_0 value increases almost linearly with the increasing T_{T1}^{in} for all the studied concepts.



411
412
413
414

Figure 9. Overall energy efficiency (η_0) as a function of the steam inlet temperature of the turbine T1 ($H_C=11$ h; $H_D=13$ h).

However, an excessive increase of T_{T1}^{in} may cause the turbine damage. Moreover, higher T_{T1}^{in} requires higher HTF temperature of the solar circuit during the charging and the higher reaction temperature of the TCS reactor during the discharging. Since the equilibrium temperature of Ca(OH)_2 synthesis is related to the pressure (e.g., 540 °C at 0.2 MPa) [Schaube 2012; Zhang 2016], the TCS reactor may have to be pressurized to render higher reaction temperature. This imposes a higher requirement on the TCS reactor design and operation as well as the more complicated control strategy for the whole installation. As a result, $T_{T1}^{in}=480$ °C (500 °C, 0.1 MPa for the TCS reactor) is selected as an appropriate operational parameter.

423
424

- TCS reactor efficiency γ

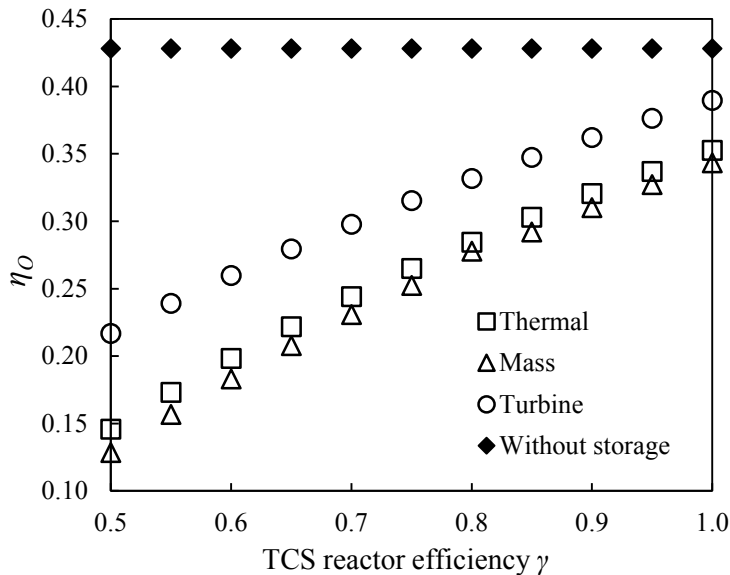
Another influencing factor is the reactor's efficiency, which is defined as the ratio of the effective heat released to the theoretical reaction heat for discharging, or the ratio of the theoretical heat needed to the effective heat absorbed for charging. This factor is closely linked with various aspects including the structure and size of the reactor, the reversibility of the TCS reaction and the chemical stability of the stored materials. Since it is difficult at this stage to quantify the respective impact of each aspect, we introduce the parameter γ as the *global TCS reactor efficiency* taking all

433 the related effects into account. We also assume identical γ for charging and for discharging, as
 434 indicated in Table 1. Note that the assumption of constant and identical γ values may not be
 435 appropriate in real practice, since the reversibility of the CaO/Ca(OH)₂ pair will decrease with the
 436 increasing number of operation cycles.

437

438 Figure 10 shows the calculated results of η_0 as a function of the global TCS reactor efficiency
 439 γ . It can be observed that the η_0 value decreases with the reduced global reactor efficiency. When γ
 440 of the TCS reactor drops from 1.0 to 0.8, the η_0 value decreases about 5% for Turbine Int., and
 441 about 7% for Mass Int. and for Thermal Int. Turbine Int. concept still has the best overall energy
 442 efficiency.

443



444

445 Figure 10. Overall energy efficiency (η_0) as a function of the TCS reactor efficiency γ ($H_c=11$ h; $H_D=13$ h).

446

447 Besides the negative impact on the overall energy efficiency, the losses that we studied will
 448 also increase the amount of storage materials needed, thus requiring a larger size of the TCS reactor
 449 for their storage and operation. In real world engineering, special attention should be given to avoid
 450 or minimize the losses to a lower limit.

451

452

453 4.3. Comparison of 3 proposed integration concepts

454

455 The parametric study carried out in section 4.2 permits evaluating the impacts of some
 456 influencing factors on the overall energy efficiency and determining more realistic operational
 457 conditions with respect to the ideal conditions used for performance modelling in section 4.1. Based
 458 on the results obtained, a comparison of the three proposed integration concepts under more realistic
 459 operational conditional is presented in Table 2. Note that detailed values of various parameters are
 460 obtained under the assumptions of $\eta_{isen}=0.85$, $T_{T1}^{in}=480$ °C, $\gamma=0.95$, $W_{T1,C(D)}=100$ MW and
 461 round-clock operation ($H_c=11$ h; $H_D=13$ h).

462

463 A size estimation of the TCS unit has been made and the results are recapitulated in Table
464 2. It is shown that the Thermal Int. concept needs a smaller quantity of TCS material (9571 t) than
465 the Mass Int. (10013 t) and the Turbine Int. (9998 t) for 13 hours discharging time. It is because the
466 water vapor from the TCS reactor is stored as saturated liquid (100 °C, 0.1 MPa) for the Thermal
467 Int. whereas for Mass Int. and Turbine Int. concepts, the water is stored at 41.5 °C. Therefore, a bit
468 more quantity of TCS materials is needed for the latter two concepts to compensate this temperature
469 difference.

Table 2. Comparison on the energy performance of three proposed integration concepts under more realistic operating conditions ($\eta_{isen}=0.85$, $T_{T1}^{in} = 480$ °C, $\gamma=0.95$, $W_{T1,C(D)} = 100$ MW and round-clock operation ($H_c=11$ h; $H_d=13$ h).

	η_o	Operational data			Heat exchange rate						Work exchange rate			Size of storage unit		
		$m_{Rankine}$ (kg·s ⁻¹)	m_{TCS} (kg·s ⁻¹)	y	SG (MW)	CON1 (MW)	CON2 (MW)	HX2 (MW)	HX1 (MW)	R (MW)	T1 (MW)	T2 (MW)	P1+2+3 (MW)	Mass of water stored (t)	Mass of CaO stored (t)	
Thermal Int.	Discharging	0.295	144	80	0.67	-	78.0	-	181.4	-	378.7	100	-	1.0	3079	9571
	Charging		91	95	0	190.8	188.7	194.4	-	97.3	548.3	100	-	0.6		
Mass Int.	Discharging	0.286	151	84	0.72	-	87.0	-	210.3	-	396.2	100	-	1.0	3221	10013
	Charging		91	99	0	187.1	188.8	228.3	-	121.2	573.7	100	-	0.6		
Turbine Int.	Discharging	0.327	151	84	0.72	-	87.1	-	210.0	-	395.6	100	-	1.50	3217	9998
	Charging		102	92	0.20	268.3	169.4	251.4	-	-	531.6	100	53.7	1.0		

462 The energy storage density is roughly estimated to be about $100 \text{ kWh}_{\text{el}} \cdot \text{t}^{-1}$. This value is
463 about seven times higher than that of existing CSP plants using molten salt as energy storage media
464 (eg. for Andasol Spain, the heat reservoir consists of two tanks measuring 14 m in height and 36 m
465 in diameter and containing 28500 tons of molten salts, enough to run the turbine for about 7.5 hours
466 at 50 MW_{el} [Pelay 2017b]). The energy storage density is calculated to be $13.1 \text{ kWh}_{\text{el}} \cdot \text{t}^{-1}$). Higher
467 energy storage density implies more compact storage unit and less heat loss of the storage reservoirs.
468

469 A first comparison between the three proposed integration concepts can then be made.
470 Firstly, the Turbine Int. concept is the most interesting ($\eta_0=0.327$) in terms of overall energy
471 efficiency. However, a second turbine is needed, implying the higher initial cost. Particular attention
472 should be given to the purity of steam leaving the TCS reactor that may cause the mechanical failure
473 of the second turbine. Efficient filtration measures are indispensable for dust removal as has been
474 discussed above. Secondly, the Mass Int. concept is the least attractive ($\eta_0=0.286$). In fact, the
475 mixing of working fluids between principal Rankine circuit and the TCS circuit may not be a good
476 option again due to the purity issue that could be vital to the turbine. Finally, the Thermal Int.
477 concept does not possess the highest overall energy efficiency, but its simple and robust design makes
478 it relatively easy towards implementation. Moreover, relatively small volumes of reservoirs are
479 required based on the size estimation reported above.
480

482 5. Exergy analysis of different TCS integration concepts

484 The previous section presents a comparison of the three proposed integration concepts based
485 on the energy analysis (first law of thermodynamics). Meanwhile, an exergy balance will also be
486 beneficial by providing supplemental insights on the quality of the energy, taking the irreversibility
487 notion of the processes into account [Dincer 2002; Rosen 2003; Kang 2018]. The main purpose of
488 this section is hence to evaluate and compare the overall exergy efficiency of the three proposed
489 integration concepts through an exergy analysis. Note that the exergy analysis and the modelling
490 results presented hereafter are obtained under realistic operating conditions ($\eta_{isen}=0.85$ and $\gamma=0.95$)
491 as specified in sections 4.3.

494 5.1. Performance modelling for the exergy analysis

496 Exergy as a thermodynamic notion means the maximum work extracted from a stream as
497 the stream reaches the dead state [Bejan, 1988]. The total exergy of a system *Ex* includes four
498 components, namely physical exergy, kinetic exergy, potential exergy and chemical exergy [Rosen
499 2003]. Neglecting the potential and kinetic exergy changes, the exergy balance of different
500 components may be modelled as follows.

- 502 • *Turbine or pump*

$$503 l = mT_0 \cdot \Delta s \quad (33)$$

$$\varepsilon = 1 - \dot{l}/(Ex_{in} + m\Delta h) \quad (34)$$

504

- *Heat exchanger*

506

$$\dot{l} = -(\Delta \dot{E}x_{hot} + \Delta \dot{E}x_{cold}) \quad (35)$$

$$\varepsilon = 1 - \dot{l}/(\dot{E}x_{hot in} + \dot{E}x_{cold in}) \quad (36)$$

507

- *Steam generator or condenser*

509

$$l = mT_0\Delta s + \frac{T_0}{T}Q \quad (37)$$

$$\varepsilon = 1 - \dot{l}/Ex_{in} \quad (38)$$

510

- *TCS reactor*

512

$$\dot{l}_R = \sum \dot{E}x_{in\,tot} - \sum \dot{E}x_{out\,tot} - (\sum \dot{l}_{tot} - \dot{l}_R) \quad (39)$$

513

Where h ($\text{J}\cdot\text{kg}^{-1}$) is the specific enthalpy, \dot{Ex} (W) the exergy and s ($\text{J}\cdot\text{K}^{-1}\cdot\text{kg}^{-1}$) the specific entropy. \dot{l} (W) is the exergy destruction of the component and ε is the exergy efficiency of the component. The overall exergy efficiency of the CSP plant η_{ex} is defined as the ratio of the exergy extracted by turbine(s) to the amount of exergy provided by the HTF of the solar circuit.

518

$$\eta_{ex} = \frac{\sum \dot{E}x_{out}}{\sum \dot{E}x_{in}} \quad (40)$$

519

520

5.2. Results and discussion

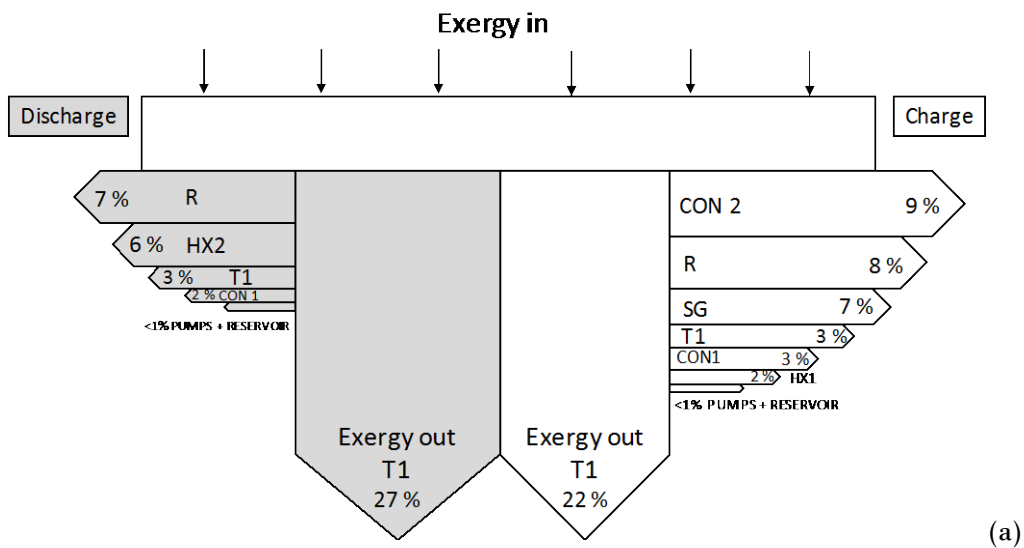
522

An exergy analysis has been performed for the three proposed integration concepts. Figure 11 shows the exergy flow-chart for each integration concept comprising of both the charging and the discharging stages. Note that the reference temperature T_0 was chosen as 5 °C, a value lower than those of the whole system. It allows an easier reading and interpretation of the results obtained.

527

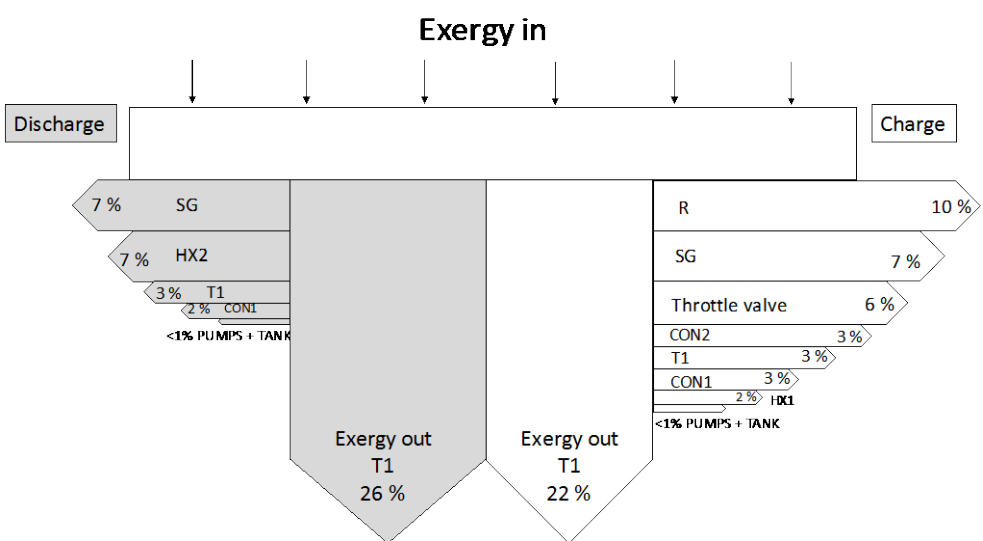
The exergy flow-chart for the Thermal Int. concept is shown in Fig. 11a, indicating that the overall exergy efficiency (η_{ex}) equals to 0.49. It can be observed that the highest exergy destructions happen in the TCS reactor and in the heat exchanger (HX2) during discharging whereas in the steam generator, in the TCS reactor and in the condenser (CON2) during charging. These exergy destructions are mainly due to the irreversibilities caused by the large amount of heat transfer in these components. Note that exergy destructions in the reservoir and in pumps are negligible. A close look at each component indicates that the CON2 with a very low exergy efficiency ($\varepsilon_{CON2}=0.19$) during charging stage is the main cause of exergy destruction.

536



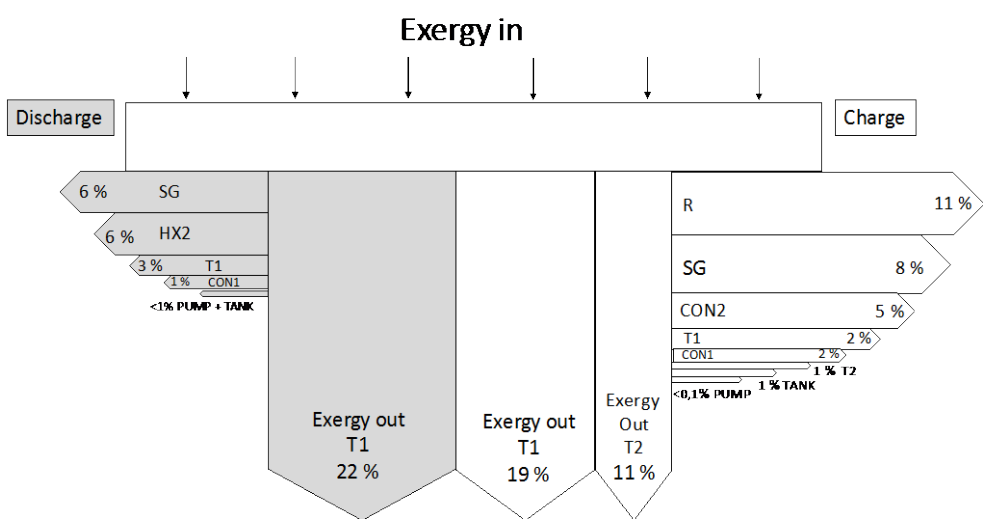
537

538



539

540



541

542

543

Figure 11. Exergy flow-chart and overall exergy efficiency (η_{ex}) for three proposed integration concepts. (a) Thermal integration concept; (b) Mass integration concept; (c) Turbine integration concept.

544

545 The Mass Int. concept has a slightly lower η_{ex} value (0.48). It can be observed from Fig. 11b
546 that the TCS reactor is the main component of exergy destruction during charging and discharging.
547 The HX2 during discharging, the SG and throttle valve (TV) during charging also have high exergy
548 destructions compared to those in reservoirs or pumps. Similar to the Thermal Int. concept, these
549 losses are mainly due to the irreversibilities caused by the large amount of heat transfer in these
550 components. An option to improve the ε_{TV} is to release the fluid at a pressure higher than 0.008
551 MPa. Nevertheless, the condensed water should be stored separately instead of sharing a common
552 reservoir which is the distinguishing feature of the Mass Int. concept.

553

554 The Turbine Int. concept has the highest exergy efficiency ($\eta_{ex}=0.52$) among the three.
555 Figure 11c indicates that the highest exergy destructions happen in the TCS reactor and in the HX2
556 during discharging whereas in the TCS reactor, in the SG and in the CON2 during charging. The
557 TCS reactor represents the highest exergy destruction of the system while the CON2 has the lowest
558 exergy efficiency ($\varepsilon_{CON2}=0.27$).

559

560 In brief, the exergy analysis of the three proposed integration concepts confirms that, in
561 terms of overall exergy efficiency of the installation, the Turbine Int. concept is the most attractive
562 ($\eta_{ex}=0.52$), followed by the Thermal Int. concept ($\eta_{ex}=0.49$) and then the Mass Int. concept
563 ($\eta_{ex}=0.48$).

564

565

566 **6. Conclusion and prospects**

567

568 This paper presents a conceptual study of three different TCS integration concepts in a
569 Rankine cycle driven by CSP. The TCS material used in this study is the CaO/Ca(OH)₂ couple. Based
570 on the energy and exergy analyses, main conclusions could be reached as follows.

571

- 572 • Different integration concepts are feasible by coupling the TCS system with a Rankine cycle
573 and by carefully determining flow circuit configurations and working conditions for
574 charging and discharging stages.
- 575 • The overall energy efficiency of the installation under ideal conditions is evaluated to be
576 0.358 for the Thermal Int. concept, 0.349 for the Mass Int. concept and 0.392 for the Turbine
577 Int. concept, respectively ($H_c=11$; $H_D=13$). Compared to the reference case without storage,
578 the TCS integration decreases the overall energy efficiency but improves the adaptability
579 and dispatchability of CSP plants with the increased power production.
- 580 • The energy storage density using calcium hydroxide as storage media is roughly estimated
581 to be about $100 \text{ kWh}_e \cdot t^{-1}$; this value is about seven times higher than that of existing CSP
582 plant with a sensible heat storage using molten salt (about $13.1 \text{ kWh}_e \cdot t^{-1}$).

583

584

585

- Different types of losses would cause a reduced overall energy efficiency of the installation. Non-isentropic compression/expansion and poor efficiency of the TCS reactor would have significant negative impacts on the overall energy efficiency.
- Among the three proposed integration concepts, the Turbine Int. concept seems to be the best option with the highest overall energy and exergy efficiencies under the tested conditions.

It should be noted that this study has focused on the integration conception issue, and promising findings have been obtained for this essential step. Nevertheless, a number of scientific & technological barriers remain to be overcome for the real implementation of TCS systems in CSP plants. Our ongoing work includes the dynamic simulation of each individual components (including the solar receiver and the TCS reactor) and the whole installation under real conditions. The techno-economic considerations in TCS evaluation are also our study focus, so as to assess the feasibility of such TCS integration into a real CSP plant. The results obtained on these remaining issues will be presented in future papers.

Acknowledgement

This work was supported by the French ANR within the project In-STORES (ANR-12-SEED-0008). The authors also wish to thank the colleagues of laboratory PROMES (CNRS UPR 8521) also involved in this ANR project, for fruitful and inspiring discussions.

Nomenclature

Latin letters

$\dot{E}x$	exergy, W
H	charging or discharging time, h
h	specific enthalpy, $\text{kJ}\cdot\text{kg}^{-1}$
\dot{l}	exergy destruction, W
m	mass flowrate, $\text{kg}\cdot\text{s}^{-1}$
n	number of mole
P	pressure, Pa
Q	heat exchange rate, W
s	specific entropy, $\text{kJ}\cdot\text{kg}^{-1}\cdot\text{K}^{-1}$
T	temperature, $^{\circ}\text{C}$
T_0	reference temperature, 5°C
W	work exchange rate, W
x	mass fraction of vapor

629 y fraction of extracted steam
630 X, Y intermediate points for the modeling of HX1

631

632

633 *Greek symbols*

634 γ global reactor efficiency
635 ε exergy efficiency of component
636 Δh_R reaction heat, $\text{kJ}\cdot\text{kg}^{-1}$
637 η_o overall energy efficiency
638 η_{isen} isentropic efficiency of turbine and pumps
639 η_{ex} overall exergy efficiency

640

641

642 *Subscripts/superscripts*

643 C charging stage
644 D discharging stage
645 el electricity
646 ext extraction
647 in inlet
648 isen isentropic
649 out outlet
650 steam steam
651 th thermal
652 tot total

653

654

655 *Abbreviation*

656 CON condenser
657 CSP concentrating solar power
658 FH feedwater heater
659 HTF heat transfer fluid
660 HX heat exchanger
661 Int. integration
662 P pump
663 PCM phase change material
664 R reactor
665 Rankine Rankine circuit
666 SG steam generator
667 T turbine
668 TCS thermochemical energy storage
669 TES thermal energy storage
670 TV throttle valve
671 WS water reservoir

672 **References**

- 673
674 Alva, G., Lin, Y., & Fang, G. (2018). An overview of thermal energy storage systems. *Energy*, 144, 341-378.
675 <https://doi.org/10.1016/j.energy.2017.12.037>
- 676
677 Álvarez De Miguel, S., Gonzalez-Aguilar, J., & Romero, M. (2013). 100-Wh multi-purpose particle reactor for
678 thermochemical heat storage in concentrating solar power plants. *Energy Procedia*, 49, 676–683.
679 <https://doi.org/10.1016/j.egypro.2014.03.073>
- 680
681 André, L., Abanades, S., & Flamant, G. (2016). Screening of thermochemical systems based on solid-gas reversible
682 reactions for high temperature solar thermal energy storage. *Renewable and Sustainable Energy Reviews*, 64,
683 703-715. <https://doi.org/10.1016/j.rser.2016.06.043>
- 684
685 Aydin, D., Casey, S. P., & Riffat, S. (2015). The latest advancements on thermochemical heat storage systems.
686 *Renewable and Sustainable Energy Reviews*, 41, 356–367. <https://doi.org/10.1016/j.rser.2014.08.054>
- 687
688 Azpiazu, M. N., Morquillas, J. M., & Vazquez, A. (2003). Heat recovery from a thermal energy storage based on
689 the Ca(OH)2/CaO cycle. *Applied Thermal Engineering*, 23, 733–741. [https://doi.org/10.1016/S1359-4311\(03\)00015-2](https://doi.org/10.1016/S1359-4311(03)00015-2)
- 690
691 Bagherisereshki, E., Tran, J., Lei, F., AuYeung, N. (2018). Investigation into SrO/SrCO3 for high temperature
692 thermochemical energy storage. *Solar Energy*, 160, 85-93. <https://doi.org/10.1016/j.solener.2017.11.073>
- 693
694 Balghouthi, M., Trabelsi, S. E., Amara, M. B., Ali, A. B. H., & Guizani, A. (2016). Potential of concentrating solar
695 power (CSP) technology in Tunisia and the possibility of interconnection with Europe. *Renewable and
696 Sustainable Energy Reviews*, 56, 1227-1248. <https://doi.org/10.1016/j.rser.2015.12.052>
- 697
698 Bejan, A. (1988). *Advanced Engineering Thermodynamics*, John Wiley & Sons Inc., New York.
- 699
700 Cabeza, L. F., Gutierrez, A., Barreneche, C., Ushak, S., Fernández, Á. G., Inés Fernández, A., & Grágeda, M. (2015).
701 Lithium in thermal energy storage: A state-of-the-art review. *Renewable and Sustainable Energy Reviews*, 42,
702 1106–1112. <https://doi.org/10.1016/j.rser.2014.10.096>
- 703
704 Cabeza, L. F., Solé, A., Fontanet, X., Barreneche, C., Jové, A., Gallas, M., Fernández, A. I. (2017). Thermochemical
705 energy storage by consecutive reactions for higher efficient concentrated solar power plants (CSP): Proof
706 of concept. *Applied Energy*, 185, 836–845. <https://doi.org/10.1016/j.apenergy.2016.10.093>
- 707
708 Cáceres, G., Anrique, N., Girard, A., Degrève, J., Baeyens, J., & Zhang, H. L. (2013). Performance of molten salt
709 solar power towers in Chile. *Journal of Renewable and Sustainable Energy*, 5(5).
710 <https://doi.org/10.1063/1.4826883>
- 711
712 Calderón, A., Palacios, A., Barreneche, C., Segarra, M., Prieto, C., Rodriguez-Sánchez, A., & Fernández, A. I.
713 (2018). High temperature systems using solid particles as TES and HTF material: A review. *Applied Energy*,
714 213, 100-111. <https://doi.org/10.1016/j.apenergy.2017.12.107>
- 715
716 Chase, M. W. Jr. (1998). *NIST-JANAF Thermochemical Tables, Fourth Edition*. Journal of Physical and Chemical
717 Reference Data.
- 718
719 Chirino, H., Xu, B., Xu, X., & Guo, P. (2018). Generalized diagrams of energy storage efficiency for latent heat
720 thermal storage system in concentrated solar power plant. *Applied Thermal Engineering*, 129, 1595–1603.
721 <https://doi.org/10.1016/j.applthermaleng.2017.10.153>
- 722
723 del Río, P., Peñasco, C., & Mir-Artigues, P. (2018). An overview of drivers and barriers to concentrated solar
724 power in the European Union. *Renewable and Sustainable Energy Reviews*, 81, 1019-1029.
725 <https://doi.org/10.1016/j.rser.2017.06.038>
- 726
727 Deutsch, M., Horvath, F., Knoll, C., Lager, D., Gierl-Mayer, C., Weinberger, P., & Winter, F. (2017). High-
728 Temperature Energy Storage: Kinetic Investigations of the CuO/Cu₂O Reaction Cycle. *Energy & Fuels*,
729 31(3), 2324–2334. <https://doi.org/10.1021/acs.energyfuels.6b02343>

- 731
732 Dincer, I. (2002). Thermal energy storage systems as a key technology in energy conservation. *International Journal*
733 *of Energy Research*, 26(7), 567–588. <https://doi.org/10.1002/er.805>
- 734
735 Dowling, A. W., Zheng, T., & Zavala, V. M. (2017). Economic assessment of concentrated solar power
736 technologies: A review. *Renewable and Sustainable Energy Reviews*, 72, 1019-1032.
737 <https://doi.org/10.1016/j.rser.2017.01.006>
- 738
739 Dunham, M. T., & Iverson, B. D. (2014). High-efficiency thermodynamic power cycles for concentrated solar
740 power systems. *Renewable and Sustainable Energy Reviews*, 30, 758–770.
741 <https://doi.org/10.1016/j.rser.2013.11.010>
- 742
743 Dunn, R. I., Hearps, P. J., & Wright, M. N. (2012). Molten-salt power towers: Newly commercial concentrating
744 solar storage. In *Proceedings of the IEEE* (Vol. 100, pp. 504–515).
745 <https://doi.org/10.1109/JPROC.2011.2163739>
- 746
747 Fernandes, D., Pitié, F., Cáceres, G., & Baeyens, J. (2012). Thermal energy storage: “How previous findings
748 determine current research priorities.” *Energy*, 39(1), 246–257. <https://doi.org/10.1016/j.energy.2012.01.024>
- 749
750 Gil, A., Medrano, M., Martorell, I., Lázaro, A., Dolado, P., Zalba, B., & Cabeza, L. F. (2010). State of the art on
751 high temperature thermal energy storage for power generation. Part I-Concepts, materials and
752 modellization. *Renewable and Sustainable Energy Reviews*, 14, 31-55. <https://doi.org/10.1016/j.rser.2009.07.035>
- 753
754 Gutierrez, A., Miró, L., Gil, A., Rodríguez-Aseguinolaza, J., Barreneche, C., Calvet, N., Cabeza, L. F. (2016).
755 Advances in the valorization of waste and by-product materials as thermal energy storage (TES) materials.
756 *Renewable and Sustainable Energy Reviews*, 59, 763–783. <https://doi.org/10.1016/j.rser.2015.12.071>
- 757
758 IEA (2014). Energy Technology Perspectives. París, France: IEA publications; <http://www.iea.org/etp/etp2014/>.
- 759
760 IRENA (2016). REmap: roadmap for a renewable energy future, 2016 edition. Abu Dhabi: International Renewable
761 Energy Agency (IRENA); (www.irena.org/remap).
- 762
763 Kang, Q., Dewil, R., Degrève, J., Baeyens, J., Zhang, H. (2018). Energy analysis of a particle suspension solar
764 combined cycle power plant. *Energy Conversion and Management*, 163, 293-303.
765 <https://doi.org/10.1016/j.enconman.2018.02.067>
- 766
767 Kuravi, S., Trahan, J., Goswami, D. Y., Rahman, M. M., & Stefanakos, E. K. (2013). Thermal energy storage
768 technologies and systems for concentrating solar power plants. *Progress in Energy and Combustion Science*,
769 39, 285-319. <https://doi.org/10.1016/j.pecs.2013.02.001>
- 770
771 Liu, M., Steven Tay, N. H., Bell, S., Belusko, M., Jacob, R., Will, G., Saman, W., Bruno, F. (2016). Review on
772 concentrating solar power plants and new developments in high temperature thermal energy storage
773 technologies. *Renewable and Sustainable Energy Reviews*, 53, 1411-1432.
774 <https://doi.org/10.1016/j.rser.2015.09.026>
- 775
776 Luo, L., Fan Y., Mazet, N., Stitou, D., Mauran, S., Neveu, P. (2016). Installation de production d'électricité
777 comprenant un stockage de chaleur. French Patent FR 16 62785
- 778
779 Michel, B., Mazet, N., Mauran, S., Stitou, D., & Xu, J. (2012). Thermochemical process for seasonal storage of
780 solar energy: Characterization and modeling of a high density reactive bed. *Energy*, 47, 553–563.
781 <https://doi.org/10.1016/j.energy.2012.09.029>
- 782
783 Moran, M.J., Shapiro, H.N., Munson, B.R., DeWitt, D.P., (2003). *Introduction to Thermal Systems Engineering: Thermodynamics, Fluid Mechanics and Heat Transfer*. John Wiley & Sons, Inc.
- 784
785 Myers, P. D., & Goswami, D. Y. (2016). Thermal energy storage using chloride salts and their eutectics. *Applied Thermal Engineering*, 109, 889–900. <https://doi.org/10.1016/j.applthermaleng.2016.07.046>
- 786
787
788

- 789 Nithyanandam, K., & Pitchumani, R. (2014). Cost and performance analysis of concentrating solar power systems
790 with integrated latent thermal energy storage. *Energy*, 64, 793–810.
791 <https://doi.org/10.1016/j.energy.2013.10.095>
- 792
- 793 Ortega-Fernández, I., Calvet, N., Gil, A., Rodríguez-Aseguinolaza, J., Faik, A., & D'Aguanno, B. (2015).
794 Thermophysical characterization of a by-product from the steel industry to be used as a sustainable and
795 low-cost thermal energy storage material. *Energy*, 89, 601–609. <https://doi.org/10.1016/j.energy.2015.05.153>
- 796
- 797 Ortiz, C., Chacartegui, R., Valverde, J. M., Alovisio, A., & Becerra, J. A. (2017). Power cycles integration in
798 concentrated solar power plants with energy storage based on calcium looping. *Energy Conversion and
799 Management*, 149, 815–829. <https://doi.org/10.1016/j.enconman.2017.03.029>
- 800
- 801 Pan, Z. H., & Zhao, C. Y. (2017). Gas-solid thermochemical heat storage reactors for high-temperature
802 applications. *Energy*, 130, 155–173. <https://doi.org/10.1016/j.energy.2017.04.102>
- 803
- 804 Parrado, C., Cáceres, G., Bize, F., Bubnovich, V., Baeyens, J., Degrève, J., & Zhang, H. L. (2015). Thermo-
805 mechanical analysis of copper-encapsulated NaNO₃-KNO₃. *Chemical Engineering Research and Design*, 93,
806 224–231. <https://doi.org/10.1016/j.cherd.2014.07.007>
- 807
- 808 Pardo, P., Anxionnaz-Minvielle, Z., Rougé, S., Cognet, P., & Cabassud, M. (2014). Ca(OH)₂/CaO reversible
809 reaction in a fluidized bed reactor for thermochemical heat storage. *Solar Energy*, 107, 605–616.
810 <https://doi.org/10.1016/j.solener.2014.06.010>
- 811
- 812 Pardo, P., Deydier, A., Anxionnaz-Minvielle, Z., Rougé, S., Cabassud, M., & Cognet, P. (2014). A review on high
813 temperature thermochemical heat energy storage. *Renewable and Sustainable Energy Reviews*, 32, 591–610
814 <https://doi.org/10.1016/j.rser.2013.12.014>
- 815
- 816 Pelay, U., Luo, L., Fan, Y., Stitou, D., & Rood, M. (2017a). Thermal energy storage systems for concentrated solar
817 power plants. *Renewable and Sustainable Energy Reviews*, 79, 82–100.
818 <https://doi.org/10.1016/j.rser.2017.03.139>
- 819
- 820 Pelay, U., Luo, L., Fan, Y., Stitou, D., & Rood, M. (2017b). Technical data for concentrated solar power plants in
821 operation, under construction and in project. *Data in Brief*, 13, 597–599.
822 <https://doi.org/10.1016/j.dib.2017.06.030>
- 823
- 824 Pitié, F., Zhao, C. Y., Baeyens, J., Degrève, J., & Zhang, H. L. (2013). Circulating fluidized bed heat recovery/storage
825 and its potential to use coated phase-change-material (PCM) particles. *Applied Energy*, 109, 505–513.
826 <https://doi.org/10.1016/j.apenergy.2012.12.048>
- 827
- 828 Prieto, C., Cooper, P., Fernández, A. I., & Cabeza, L. F. (2016). Review of technology: Thermochemical energy
829 storage for concentrated solar power plants. *Renewable and Sustainable Energy Reviews*, 60, 909–929.
830 <https://doi.org/10.1016/j.rser.2015.12.364>
- 831
- 832 Rosen, M. A., & Dincer, I. (2003). Exergy methods for assessing and comparing thermal storage systems.
833 *International Journal of Energy Research*, 27(4), 415–430. <https://doi.org/10.1002/er.885>
- 834
- 835 Sakellariou, K. G., Criado, Y. A., Tsongidis, N. I., Karagiannakis, G., & Konstandopoulos, A. G. (2017). Multi-cyclic
836 evaluation of composite CaO-based structured bodies for thermochemical heat storage via the
837 CaO/Ca(OH)₂ reaction scheme. *Solar Energy*, 146, 65–78. <https://doi.org/10.1016/j.solener.2017.02.013>
- 838
- 839 Schabe, F., Koch, L., Wörner, A., & Müller-Steinhagen, H. (2012). A thermodynamic and kinetic study of the de-
840 and rehydration of Ca(OH)₂ at high H₂O partial pressures for thermo-chemical heat storage. *Thermochimica
841 Acta*, 538, 9–20. <https://doi.org/10.1016/j.tca.2012.03.003>
- 842
- 843 Schabe, F., Utz, I., Wörner, A., & Müller-Steinhagen, H. (2013a). De- and rehydration of Ca(OH)₂ in a reactor
844 with direct heat transfer for thermo-chemical heat storage. Part A: Experimental results. *Chemical
845 Engineering Research and Design*, 91, 856–864. <https://doi.org/10.1016/j.cherd.2012.09.020>
- 846

- 847 Schabe, F., Utz, I., Wörner, A., & Müller-Steinhagen, H. (2013b). De- and rehydration of Ca(OH)2 in a reactor
848 with direct heat transfer for thermo-chemical heat storage. Part B: Validation of model. *Chemical Engineering*
849 *Research and Design*, 91, 865–873. <https://doi.org/10.1016/j.cherd.2013.02.019>
- 850
- 851 Schabe, F., Wörner, A., & Tamme, R. (2011). High temperature thermochemical heat storage for concentrated
852 solar power using gas-solid reactions. *Journal of Solar Energy Engineering*, 133, 031006.
853 <https://doi.org/10.1115/1.4004245>
- 854
- 855 Schmidt, M., Gutierrez, A., & Linder, M. (2017). Thermochemical energy storage with CaO/Ca(OH)2—
856 Experimental investigation of the thermal capability at low vapor pressures in a lab scale reactor. *Applied*
857 *Energy*, 188, 672–681. <https://doi.org/10.1016/j.apenergy.2016.11.023>
- 858
- 859 Schmidt, M., & Linder, M. (2017). Power generation based on the Ca(OH)2/ CaO thermochemical storage system
860 – Experimental investigation of discharge operation modes in lab scale and corresponding conceptual
861 process design. *Applied Energy*, 203, 594–607. <https://doi.org/10.1016/j.apenergy.2017.06.063>
- 862
- 863 Sharma, R. K., Ganesan, P., Tyagi, V. V., Metselaar, H. S. C., & Sandaran, S. C. (2015). Developments in organic
864 solid-liquid phase change materials and their applications in thermal energy storage. *Energy Conversion and*
865 *Management*, 95, 193–228. <https://doi.org/10.1016/j.enconman.2015.01.084>
- 866
- 867 Smolders, K., & Baeyens, J. (2000). Cleaning of hot calciner exhaust gas by low-density ceramic filters. *Powder*
868 *Technology*, 111(3), 240–244. [https://doi.org/10.1016/S0032-5910\(99\)00291-0](https://doi.org/10.1016/S0032-5910(99)00291-0)
- 869
- 870 Tescari, S., Singh, A., De Oliveira, L., Breuer, S., Agrafiotis, C., Roeb, M., Sattler, C., Marcher, J., Pagkoura, C.,
871 Karagiannakis, G., Konstandopoulos, A. G. (2017). Experimental proof of concept of a pilot-scale
872 thermochemical storage unit. In *AIP Conference Proceedings* (Vol. 1850). American Institute of Physics Inc.
873 <https://doi.org/10.1063/1.4984455>
- 874
- 875 Tescari, S., Singh, A., Agrafiotis, C., de Oliveira, L., Breuer, S., Schlögl-Knothe, B., Roeb, M., Sattler, C. (2017).
876 Experimental evaluation of a pilot-scale thermochemical storage system for a concentrated solar power
877 plant. *Applied Energy*, 189, 66–75. <https://doi.org/10.1016/j.apenergy.2016.12.032>
- 878
- 879 Tian, Y., & Zhao, C. Y. (2013). A review of solar collectors and thermal energy storage in solar thermal
880 applications. *Applied Energy*, 104, 538–553. <https://doi.org/10.1016/j.apenergy.2012.11.051>
- 881
- 882 Tiskatine, R., Aharoune, A., Bouirden, L., & Ihlal, A. (2017). Identification of suitable storage materials for solar
883 thermal power plant using selection methodology. *Applied Thermal Engineering*, 117, 591–608.
884 <https://doi.org/10.1016/j.applthermaleng.2017.01.107>
- 885
- 886 Valverde, J. M., Barea-López, M., Perejón, A., Sánchez-Jiménez, P. E., & Pérez-Maqueda, L. A. (2017). Effect of
887 thermal pretreatment and nanosilica addition on limestone performance at calcium-looping conditions for
888 thermochemical energy storage of concentrated solar power. *Energy and Fuels*, 31(4), 4226–4236.
889 <https://doi.org/10.1021/acs.energyfuels.6b03364>
- 890
- 891 Wokon, M., Kohzer, A., & Linder, M. (2017). Investigations on thermochemical energy storage based on technical
892 grade manganese-iron oxide in a lab-scale packed bed reactor. *Solar Energy*, 153, 200–214.
893 <https://doi.org/10.1016/j.solener.2017.05.034>
- 894
- 895 Xu, B., Li, P., & Chan, C. (2015). Application of phase change materials for thermal energy storage in concentrated
896 solar thermal power plants: A review to recent developments. *Applied Energy*, 160, 286–307.
897 <https://doi.org/10.1016/j.apenergy.2015.09.016>
- 898
- 899 Yan, J., & Zhao, C. Y. (2016). Experimental study of CaO/Ca(OH)2 in a fixed-bed reactor for thermochemical
900 heat storage. *Applied Energy*, 175, 277–284. <https://doi.org/10.1016/j.apenergy.2016.05.038>
- 901
- 902 Yan, J., Zhao, C. Y., & Pan, Z. H. (2017). The effect of CO2 on Ca(OH)2 and Mg(OH)2 thermochemical heat
903 storage systems. *Energy*, 124, 114–123. <https://doi.org/10.1016/j.energy.2017.02.034>
- 904

- 905 Zhang, H. L., Baeyens, J., Degrève, J., Cáceres, G., Segal, R., & Pitié, F. (2014). Latent heat storage with tubular-
906 encapsulated phase change materials (PCMs). *Energy*, 76, 66–72.
907 <https://doi.org/10.1016/j.energy.2014.03.067>
- 908
909 Zhang, H. L., Baeyens, J., Degrève, J., & Cacères, G. (2013). Concentrated solar power plants: Review and design
910 methodology. *Renewable and Sustainable Energy Reviews*, 22, 466–481.
911 <https://doi.org/10.1016/j.rser.2013.01.032>
- 912
913 Zhang, H., Baeyens, J., Cáceres, G., Degrève, J., & Lv, Y. (2016). Thermal energy storage: Recent developments
914 and practical aspects. *Progress in Energy and Combustion Science*, 53, 1–40.
915 <https://doi.org/10.1016/j.pecs.2015.10.003>
- 916
917 Zhang, H., Benoit, H., Perez-Lopèz, I., Flamant, G., Tan, T., & Baeyens, J. (2017). High-efficiency solar
918 power towers using particle suspensions as heat carrier in the receiver and in the thermal energy
919 storage. *Renewable Energy*, 111, 438–446. <https://doi.org/10.1016/j.renene.2017.03.101>
- 920
921 Zhang, H., Huys, K., Baeyens, J., Degrève, J., Kong, W., & Lv, Y. (2016). Thermochemical energy storage
922 for power generation on demand. *Energy Technology*, 4(2), 341–352.
923 <https://doi.org/10.1002/ente.201500261>
- 924 Zhang, H., Kong, W., Tan, T., & Baeyens, J. (2017b). High-efficiency concentrated solar power plants
925 need appropriate materials for high-temperature heat capture, conveying and storage. *Energy*,
926 139, 52–64. <https://doi.org/10.1016/j.energy.2017.07.129>
- 927
928
929
930